







A Systematic Observational Study on Galactic Interstellar Ratio $^{18}\text{O}/^{17}\text{O}$. II. C^{18}O and C^{17}O J=2-1 Data Analysis

Y. P. ZOU (邹益鹏) ¹, J. S. ZHANG (张江水) ¹, C. HENKEL ^{2,3,4}, D. ROMANO ⁵, W. LIU (刘玮)¹,
Y. H. ZHENG (郑映慧) ^{6,7}, Y. T. YAN (闫耀庭)², J. L. CHEN (陈家梁) ¹, Y. X. WANG (汪友鑫)¹ AND
J. Y. ZHAO (赵洁瑜)¹

¹Center for Astrophysics, Guangzhou University, Guangzhou, 510006, People's Republic of China

²Max-Planck-Institut für Radioastronomie, Auf dem Hügel 69, D-53121 Bonn, Germany

³Astronomy Department, King Abdulaziz University, P.O. Box 80203, 21589 Jeddah, Saudi Arabia

⁴Xinjiang Astronomical Observatory, Chinese Academy of Sciences, 830011 Urumqi, Peoples Republic of China

⁵INAF, Osservatorio di Astrofisica e Scienza dello Spazio, Via Gobetti 93/3, I-40129 Bologna, Italy

⁶National Astronomical Observatories, Chinese Academy of Sciences, Beijing, China

⁷University of Chinese Academy of Sciences, Beijing, China

ABSTRACT

To investigate the relative amount of ejecta from high-mass versus intermediate-mass stars and to trace the chemical evolution of the Galaxy, we have performed with the IRAM 30 m and the SMT 10 m telescopes a systematic study of Galactic interstellar $^{18}\text{O}/^{17}\text{O}$ ratios toward a sample of 421 molecular clouds, covering a galactocentric distance range of $\sim 1 - 22$ kpc. The results presented in this paper are based on the J=2-1 transition and encompass 364 sources showing both C^{18}O and C^{17}O detections. The previously suggested $^{18}\text{O}/^{17}\text{O}$ gradient is confirmed. For the 41 sources detected with both facilities, good agreement is obtained. A correlation of $^{18}\text{O}/^{17}\text{O}$ ratios with heliocentric distance is not found, indicating that beam dilution and linear beam sizes are not relevant. For the subsample of IRAM 30 m high-mass star-forming regions with accurate parallax distances, an unweighted fit gives $^{18}\text{O}/^{17}\text{O} = (0.12 \pm 0.02)R_{GC} + (2.38 \pm 0.13)$ with a correlation coefficient of $R = 0.67$. While the slope is consistent with our J=1-0 measurement, ratios are systematically lower. This should be caused by larger optical depths of C^{18}O 2-1 lines, w.r.t the corresponding 1-0 transitions, which is supported by RADEX calculations and the fact that $\text{C}^{18}\text{O}/\text{C}^{17}\text{O}$ is positively correlated with $^{13}\text{CO}/\text{C}^{18}\text{O}$. After considering optical depth effects with C^{18}O J=2-1 reaching typically an optical depth of ~ 0.5 , corrected $^{18}\text{O}/^{17}\text{O}$ ratios from the J=1-0 and J=2-1 lines become consistent. A good numerical fit to the data is provided by the MWG-12 model, including both rotating stars and novae.

Keywords: Interstellar molecules (849); Radio sources (1357); Isotopic abundances (867); Galaxy chemical evolution (580)

1. INTRODUCTION

The evolution of metallicity in the Galactic disk is the consequence of stellar nucleosynthesis, which converts hydrogen to heavier elements, which are subsequently ejected into the interstellar medium (ISM; e.g., Wilson & Rood 1994). The presence of Galactic radial metallicity gradients in various objects, such as stars (e.g., Xiang et al. 2017), H II regions (e.g., Esteban & Garc í a-Rojas 2018), and planetary nebulae (e.g., Henry et al. 2010), supports the inside-out formation scenario of our Galaxy (Larson 1976). Isotope abundance ratios serve as particularly suitable tracers for nucleosynthesis and stellar ejecta, because they are not only addressing overall elemental abundances but are focusing instead on specific isotopes. These can be effectively measured by observations of molecular clouds in the radio, mm-

and submm-bands, through the analysis of molecular species with more than one stable isotopologue (e.g., Yan et al. 2019; Humire et al. 2020; Yu et al. 2020; Chen et al. 2021; Yan et al. 2023).

Observing specific isotopes, the interstellar $^{18}\text{O}/^{17}\text{O}$ ratio is one of the most useful tracers of nuclear processing and metal enrichment. It is widely accepted that ^{18}O and ^{17}O have different nucleosynthetic paths. Briefly, ^{18}O is primarily synthesized in massive stars, while ^{17}O is predominantly ejected by intermediate mass stars through a longer production timescale. This can lead to a mildly positive gradient of $^{18}\text{O}/^{17}\text{O}$ along the disk, assuming an inside-out formation scenario for our Galaxy (see detailed description in Zhang et al. 2020). Recent theoretical results mainly based on numerical calculations suggest a complex interdependence of the yields on mass, metallicity and rotation of the stars. The resulting large uncertainties require observational data to constrain such models.

$^{18}\text{O}/^{17}\text{O}$ ratios can be readily determined from $\text{C}^{18}\text{O}/\text{C}^{17}\text{O}$ line intensity ratios (see details, e.g., Zhang et al. 2007). Previous measurements on the isotopic ratio were mainly performed toward individual sources (e.g., Bensch et al. 2001; Ladd 2004; Wouterloot et al. 2005; Zhang et al. 2007) or small samples (Penzias 1981; Wouterloot et al. 2008). Measured results of $^{18}\text{O}/^{17}\text{O}$ seems to be contradictive, one uniform value between the Galactic center (GC) and disk molecular clouds (Penzias 1981) or a radial gradient along the galactic disc (Wouterloot et al. 2008). A large sample is really important to determine the ratio and its possible trend, especially more data from the GC region and far outer parts of the Galaxy.

Therefore, we started a systematic observational study based on the $^{18}\text{O}/^{17}\text{O}$ isotope ratio, measuring rotational transitions of C^{18}O and C^{17}O . Our earlier work indicated lower abundance ratios in the GC region compared to molecular clouds in the Galactic disk, based on mapping toward GC molecular clouds and a single-pointing pilot survey of Galactic disk molecular clouds (Zhang et al. 2015; Li et al. 2016). The first article in our series of $^{18}\text{O}/^{17}\text{O}$ studies involving large samples of sources was based on measurements of the $J = 1-0$ lines of C^{18}O and C^{17}O (Zhang et al. 2020, hereafter Paper I). It confirmed the previously suggested Galactic radial gradient of $^{18}\text{O}/^{17}\text{O}$. However, one transition alone is not sufficient to account for radiative transfer effects. Reliable statistical results on the abundance ratio $^{18}\text{O}/^{17}\text{O}$ still need more transition lines to evaluate potential optical depth effects and thus to obtain more reliable isotope ratios. Here we present the so far missing $J = 2-1$ data from C^{18}O and C^{17}O . As mentioned in Paper I, our large sample includes star formation regions (SFRs) associated with IRAS sources and relatively strong CO emission ($T_A^* \gtrsim 10$ K, with kinematic distances taken from Wouterloot & Brand 1989) and high-mass star-forming regions (HMSFRs), whose distances have been accurately measured by the maser parallax method from the Bar and Spiral Structure Legacy (BeSSeL¹) Survey (Reid et al. 2014; Reid et al. 2019). Our sample includes 421 sources, covering galactocentric distances from the GC region to the far outer Galaxy (~ 22 kpc). Among them, 200 sources have accurate trigonometric parallax distance with a median relative uncertainty of less than 10% (according to their measured parallax data). The observations with the IRAM 30 m and the SMT 10 m are described in Section 2, the data reduction and corresponding results are presented in Section 3, while Section 4 contains an analysis and the discussion. Main results are summarized in Section 5.

2. OBSERVATIONS

2.1. IRAM 30 m observations

Our observations of the C^{18}O and C^{17}O $J=2-1$ lines were carried out from 2017, Jan. 11 till Jan. 17, using the IRAM 30 m, at the Pico Veleta Observatory (Granada, Spain). The center frequencies were set at 219.560354 and 224.714187 GHz for the C^{18}O and C^{17}O lines, respectively. The observations were performed in position switching mode with the off position $30'$ from the source. Using the Eight Mixer Receiver (EMIR) with dual-polarization and the Fourier Transform Spectrometers (FTS) backend, a frequency coverage of 218-226 GHz in the lower sideband was obtained, with a spectral resolution of 195 kHz (corresponding to a velocity resolution of 0.26 km s^{-1}) around 222 GHz. The system temperature was about 250 K with an rms noise range in the resulting spectra of 21-119 mK with a median value of 38 mK on the antenna temperature scale T_A^* . Antenna temperatures can be transformed, multiplied by the ratio of the forward hemisphere efficiency and the main beam efficiency ($F_{eff}/B_{eff} \sim 0.92/0.59 = 1.56^2$) into main beam brightness temperatures, T_{mb} .

With the IRAM 30 m, we observed 103 sources of our sample. Observational parameters are summarized in Table 1. The source name and its equatorial J2000 coordinates are listed in Columns 1-3. The galactocentric and heliocentric

¹ <http://bessel.vlbi-astrometry.org/>

² <https://publicwiki.iram.es/Iram30mEfficiencies>

distance of each source, the telescope used, and targeted molecular species are listed in Columns 4-7. Column 8 provides the rms noise of observations, Column 9 is the velocity of the peak T_{mb} , and Columns 10 and 11 list the integrated line intensity and the peak temperature, respectively, obtained from Gaussian fits to the spectra. For each source the results for C¹⁸O are on the first and those of C¹⁷O are on the second line. Column 12 presents the abundance ratios (see details in Section 3).

2.2. SMT 10 m observations

Our SMT 10 m (on Mt. Graham, AZ, USA) observations of J=2-1 lines were performed remotely in 2016 May and June, 2018 January and November, 2019 December, 2020 June, July and November, as well as 2021 January and February with a beam size of $\sim 29''$. A dual-polarization 1.3 mm receiver frontend and the SMT 10 m filter bank backends in the 2 IF mode were used, which provide bandwidths of 1000 and 256 MHz and spectral resolutions of 1000 and 250 kHz (corresponding to velocity resolutions of 1.32 and 0.33 km s⁻¹, respectively. The latter was used for our analysis, in order to make comparisons with IRAM 30 m data). A position switching mode with reference positions 30' off in azimuth was adopted. On the antenna temperature scale T_A^* , the system temperature was ~ 380 K with an rms noise range in the resulting spectra of 14-533 mK with an median value of 37 mK in our observations. The antenna temperature can be converted, divided by the main beam efficiency correction factor ($\eta_b = 0.71^3$), into main beam brightness temperature T_{mb} .

Table 1 presents the observational parameters of the SMT 10 m results for the sample of 380 sources, including those 62 observed by both the IRAM 30 m and the SMT 10 m telescopes. Comparing observational results of the same source from different telescopes is necessary to evaluate calibration uncertainties and the effect of the beam size on the line ratios.

3. DATA REDUCTION AND RESULTS

Data reduction was done using the Continuum and Line Analysis Single-dish Software (CLASS) of the Grenoble Image and Line Data Analysis Software packages (GILDAS). Baselines were subtracted with polynomial fitting. After baseline subtraction, line parameters were obtained from Gaussian fits to the C¹⁸O and C¹⁷O spectra (see green lines in Figures 1 and 2).

96 out of 103 sources were successfully detected in both C¹⁸O and C¹⁷O J=2-1 by the IRAM 30 m, while 325 out of 380 sources were detected in both lines using the SMT 10 m. Moreover, 57 out of 62 common sources observed by both telescopes were detected in both lines. To summarize, 364 sources within our sample of 421 targeted Galactic molecular clouds have been detected in both the C¹⁸O and C¹⁷O J=2-1 lines. All the detected IRAM and SMT spectra are presented in Figures 1 and 2, respectively. In addition, the spectra of those sources without effective C¹⁸O/C¹⁷O determinations are shown in the Appendix.

The abundance ratio $Ratio_{\text{corr}}$ can be determined from the integrated intensity ratio $I(\text{C}^{18}\text{O})/I(\text{C}^{17}\text{O})$ times the factor $(\nu_{\text{C}^{17}\text{O}}/\nu_{\text{C}^{18}\text{O}})^2 = 1.047$ (see description in Paper I). Our spectral fitting results, including the peak value (T_{peak}), the integrated intensities of C¹⁸O and C¹⁷O with their uncertainties, and the abundance ratios with their uncertainty, are also presented in Table 1.

³ <https://aro.as.arizona.edu/?q=beam-efficiencies>

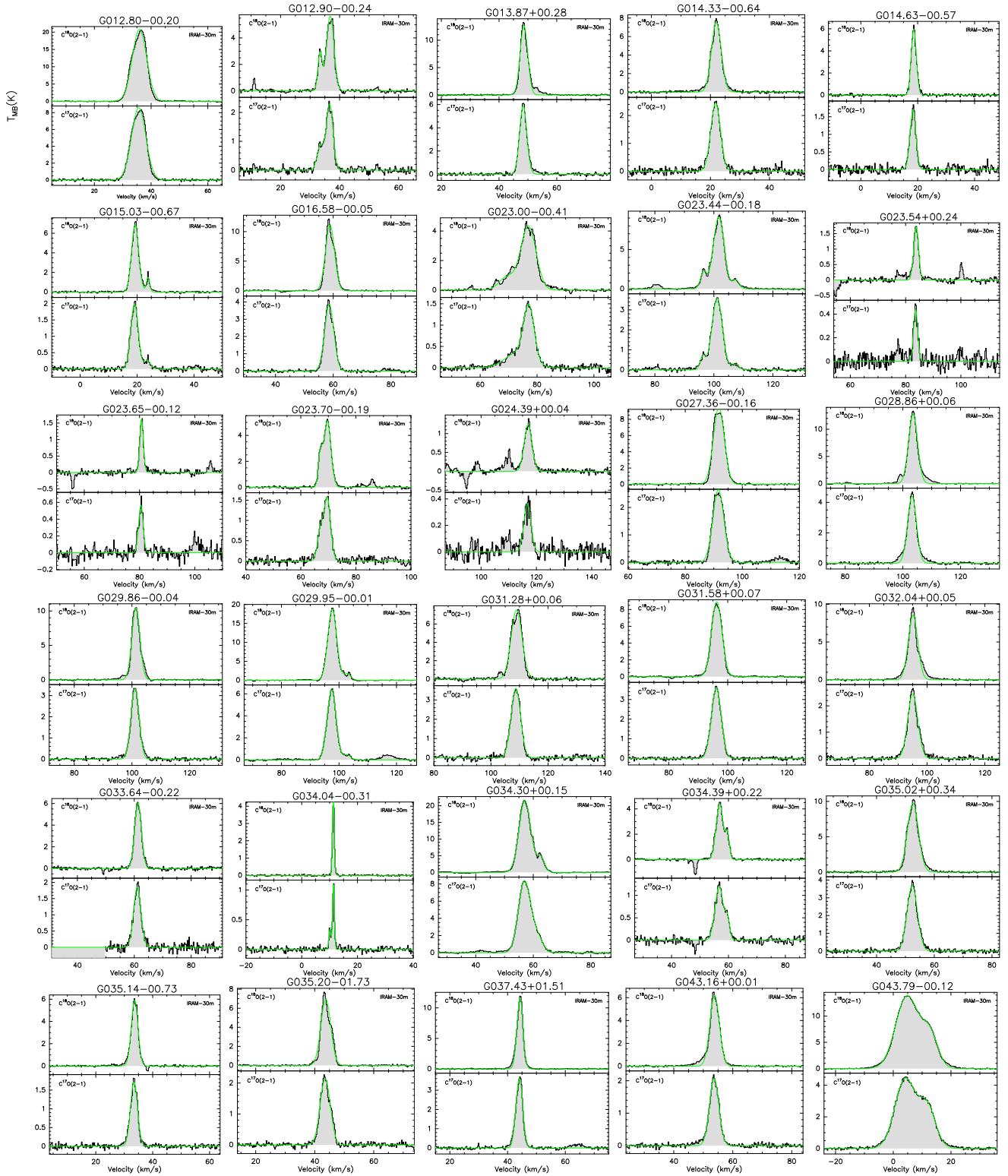


Figure 1. The IRAM 30 m spectra of C^{18}O (upper panels) and C^{17}O (lower panels) with green fit lines of the 96 sources detected in both isotopologues. (An extended version of this figure is available).

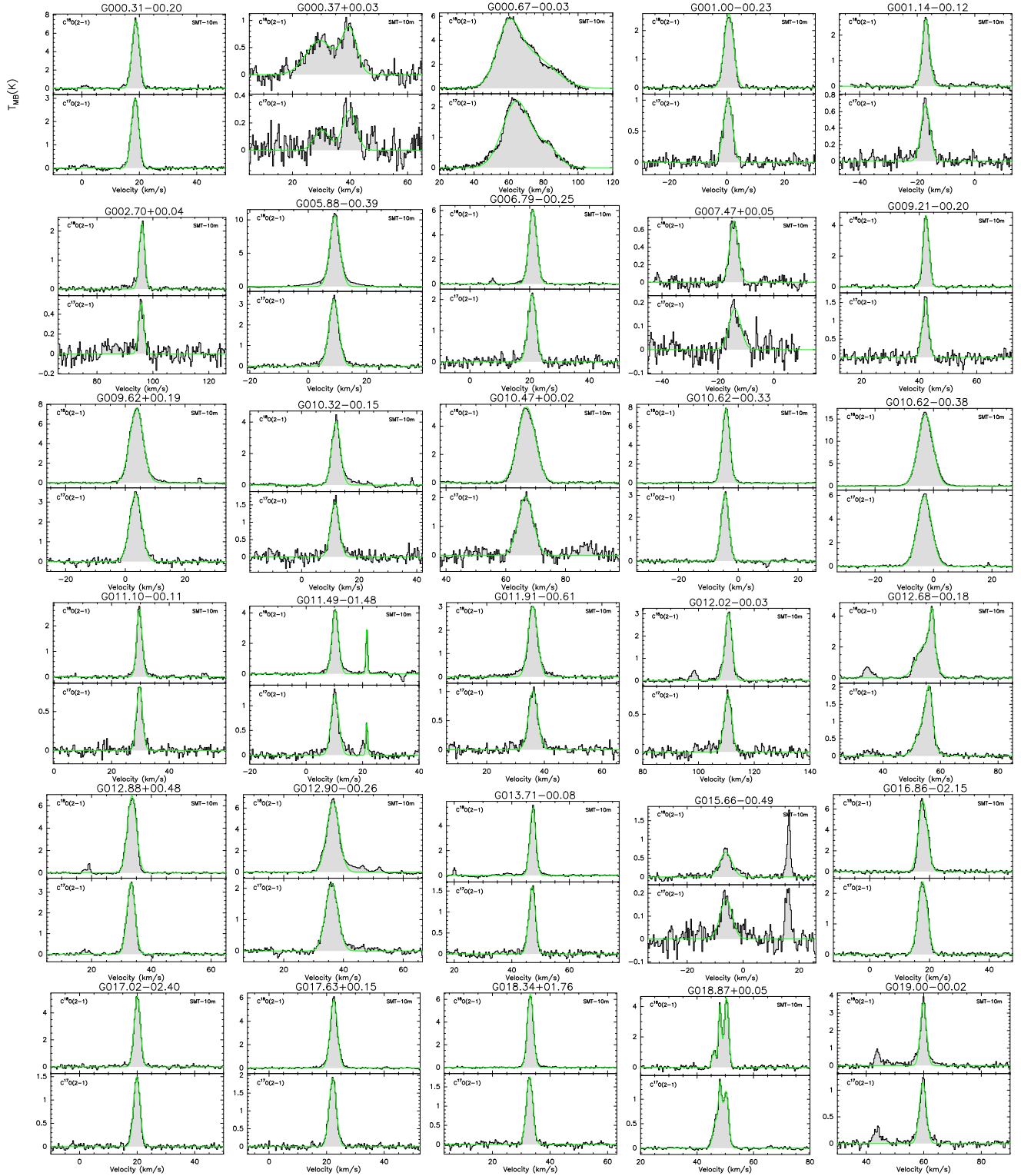


Figure 2. The SMT 10 m spectra of $C^{18}O$ (upper panels) and $C^{17}O$ (lower panels) with green fit lines of the 325 sources detected in both isotopologues. (An extended version of this figure is available).

Table 1. Observational parameters and $^{18}\text{O}/^{17}\text{O}$ isotope ratios.

Source Name	R.A.	Decl.	R_{GC}	d	Telescope	Line	rms	V_{peak}	$\int T_{mb}d\nu$	T_{peak}	$Ratio_{corr}$
(1)	(J2000)	(J2000)	(kpc)	(kpc)	(6)	(7)	(mK)	(km s^{-1})	(K km s^{-1})	(K)	(12)
WB89 312	00 02 41.3	64 34 04.01	11.39	4.60	SMT	C ^{18}O	43	-47.52 (0.02)	1.25 (0.04)	0.99	2.80 (0.21)
					SMT	C ^{17}O	23	-47.65 (0.06)	0.47 (0.03)	0.22	
WB89 325	00 14 26.6	64 28 30.29	10.57	3.39	SMT	C ^{18}O	43	-35.83 (0.01)	5.36 (0.07)	2.55	4.02 (0.12)
					SMT	C ^{17}O	29	-36.02 (0.03)	1.40 (0.04)	0.63	
WB89 326	00 15 29.1	61 14 40.99	10.76	3.69	SMT	C ^{18}O	43	-38.99 (0.01)	2.97 (0.04)	2.45	2.96 (0.10)
					SMT	C ^{17}O	26	-39.19 (0.03)	1.05 (0.03)	0.56	
WB89 330	00 20 58.1	62 40 18.01	10.78	3.66	IRAM	C ^{18}O	59	-38.99 (0.01)	2.52 (0.05)	2.59	3.83 (0.43)
					IRAM	C ^{17}O	67	-39.00 (0.04)	0.69 (0.08)	0.60	
WB89 331	00 21 19.4	63 19 19.99	11.81	5.02	IRAM	C ^{18}O	252	-51.69 (0.01)	1.98 (0.05)	2.30	4.21 (0.46)
					IRAM	C ^{17}O	79	-51.67 (0.04)	0.49 (0.05)	0.48	
WB89 336	00 26 55.8	65 10 27.80	14.07	7.72	SMT	C ^{18}O	39	-72.38 (0.03)	0.58 (0.03)	0.49	5.43 (0.97)
					SMT	C ^{17}O	18	-72.48 (0.08)	0.11 (0.02)	0.10	
WB89 344	00 33 42.0	66 49 49.01	14.25	7.87	SMT	C ^{18}O	25				
					SMT	C ^{17}O	37				
G121.29+00.65	00 36 47.3	63 29 02.18	8.86	0.93	IRAM	C ^{18}O	35	-17.50 (0.01)	14.16 (0.06)	5.17	3.24 (0.05)
					IRAM	C ^{17}O	43	-17.74 (0.02)	4.58 (0.06)	1.43	
					SMT	C ^{18}O	36	-17.48 (0.01)	10.45 (0.07)	3.95	3.48 (0.05)
					SMT	C ^{17}O	25	-17.66 (0.02)	3.14 (0.04)	1.00	

NOTE—Column (1): source name. Columns (2) and (3): equatorial J2000 coordinates. Column (4): the galactocentric distance R_{GC} . Column (5): the heliocentric distance d . Column (6): telescopes used. Column (7): molecular species. Column (8): the rms (velocity resolutions 0.26 and 0.33 km s^{-1} for IRAM and SMT, respectively) value in units of T_{mb} . Column (9): the velocity of the peak T_{mb} . Column (10): the integrated line intensity of C ^{18}O and C ^{17}O with standard deviation errors in parentheses. Column (11): the line peak values in T_{mb} . Column (12): the frequency-corrected abundance ratio with its error in parentheses. (This table is available in its entirety in machine-readable form.)

4. ANALYSIS AND DISCUSSION

4.1. Observational Effects

In [Paper I](#), we have analyzed a series of factors that may affect the ratios derived from our J=1-0 data of C ^{18}O and C ^{17}O , including observational effects and chemical and physical factors. As already mentioned in [Paper I](#), chemical fractionation can be safely neglected due to the high first ionization potential of oxygen. However, optical depth effects have to be analyzed, since the J=2-1 line of C ^{18}O normally shows a larger optical depth than its J=1-0 counterpart in a wide range of physical conditions ([Wouterloot et al. 2008](#)). We will check the degree of saturation in the C ^{18}O J=2-1 line and assess its possible effect on our ratio results in [Section 4.2.2](#). Here we investigate other potential biases related to our J = 2-1 data, following the analysis of the J = 1-0 data in [Paper I](#).

In [Figure 3](#), the isotopic ratios are plotted against heliocentric distance to investigate effects related to distance, i.e., to biases in beam dilution. No systematic dependence can be found, as in our J=1-0 data. This implies that the linear resolution of our data is not playing an important role, suggesting negligible small scale variations within the individual sources.

A related analysis has been carried out making use of those sources measured by both the IRAM 30 m and the SMT 10 m telescopes, involving beam sizes of $\sim 10''$ and $\sim 29''$, which correspond to a ratio in covered areas by almost an order of magnitude. Here we also have to note that C ^{18}O and C ^{17}O were measured simultaneously by the IRAM 30

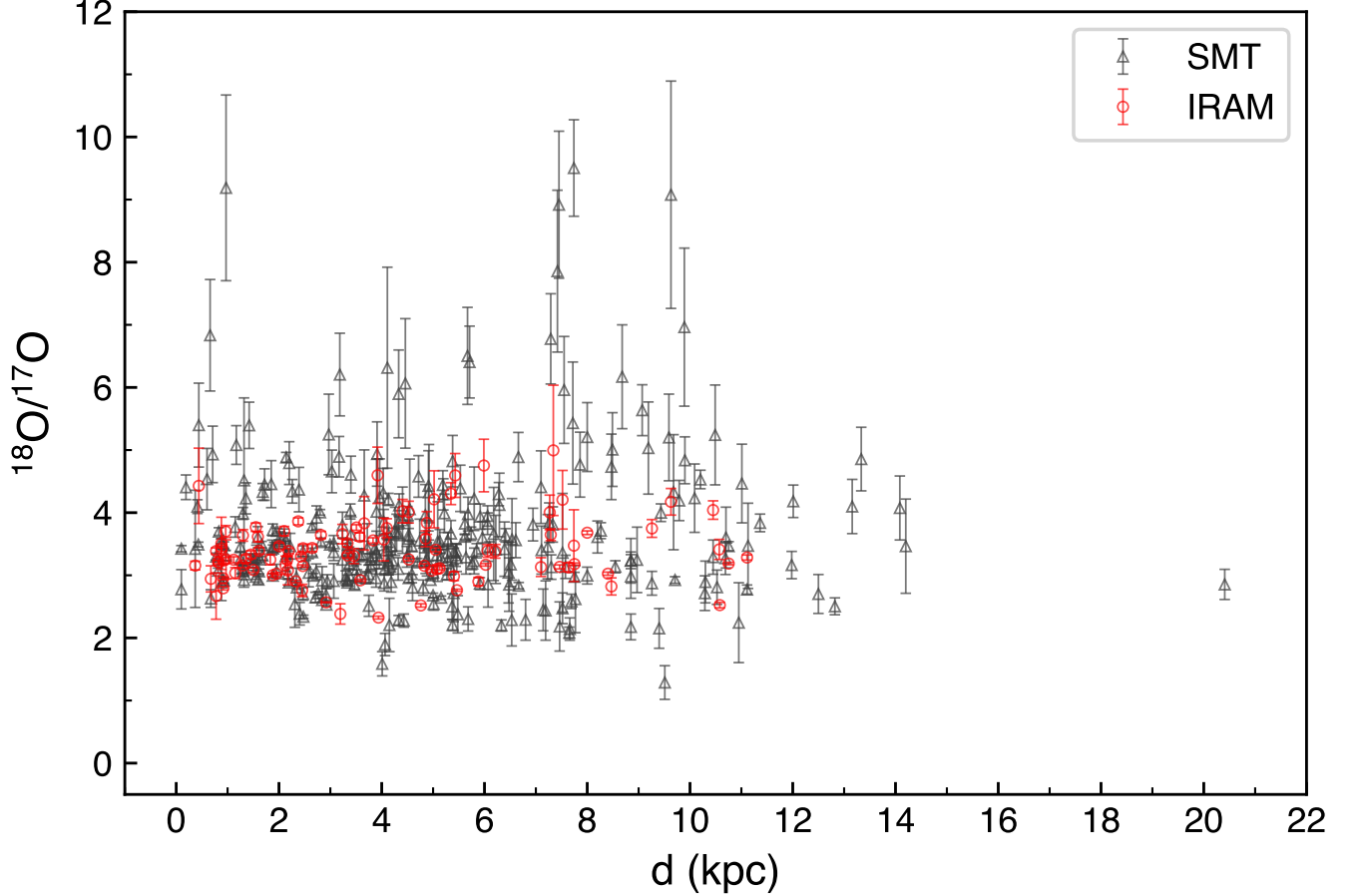


Figure 3. Abundance ratios of the entire sample plotted against heliocentric distance. Red circles and black triangles represent our IRAM 30 m and SMT 10 m measurements, respectively.

m (thanks to its broad bandwidth of ~ 8 GHz) but were observed separately by the SMT 10 m (due to its narrow bandwidth of ~ 0.25 GHz). Different observing conditions may lead to uncertainties. In case the lines are measured separately, pointing errors may affect peak and integrated intensities in different ways (Wouterloot et al. 2008). As mentioned in Section 3, 57 sources out of 62 targets are detected by both the IRAM 30 m and the SMT 10 m, which could be used to quantify these effects. The coordinates of the observed positions were taken from Reid et al. (2014); Reid et al. (2019) and Wouterloot & Brand (1989). However 16 sources had targeted position differences between both telescopes due to errors in the input coordinates for one night observation, thus only the remaining 41 sources are used for later analysis. C¹⁸O and C¹⁷O J=2-1 spectra from these 41 sources are presented in Figure 4 and the spectral fit parameters are listed in Table 2. All fitted lines detected with a smaller beam show larger main beam brightness temperatures (T_{mb}) than those from the SMT 10 m with a larger beam. This indicates that the sizes of our sources are smaller than the SMT 10 m beam size and that beam dilution is not negligible. In this case, the intensity of detected lines should be corrected for the beam dilution effect and the brightness temperatures (T_B) of the sources can be derived from the main beam brightness temperature dilution:

$$T_B = T_{\text{mb}} \frac{\theta_s^2 + \theta_{\text{beam}}^2}{\theta_s^2}, \quad (1)$$

where θ_s and θ_{beam} are source size and beam size, respectively. With Equation (1), we can estimate source size θ_s through beam sizes θ_{beam} of the two antennas and two measured T_{mb} values. Both C¹⁸O and C¹⁷O line data are employed to estimate the size of our sample. We plotted their measured source sizes from C¹⁷O lines against those from C¹⁸O lines in Figure 5(a). It is found that the estimated sizes from both lines are mostly ($>80\%$) comparable,

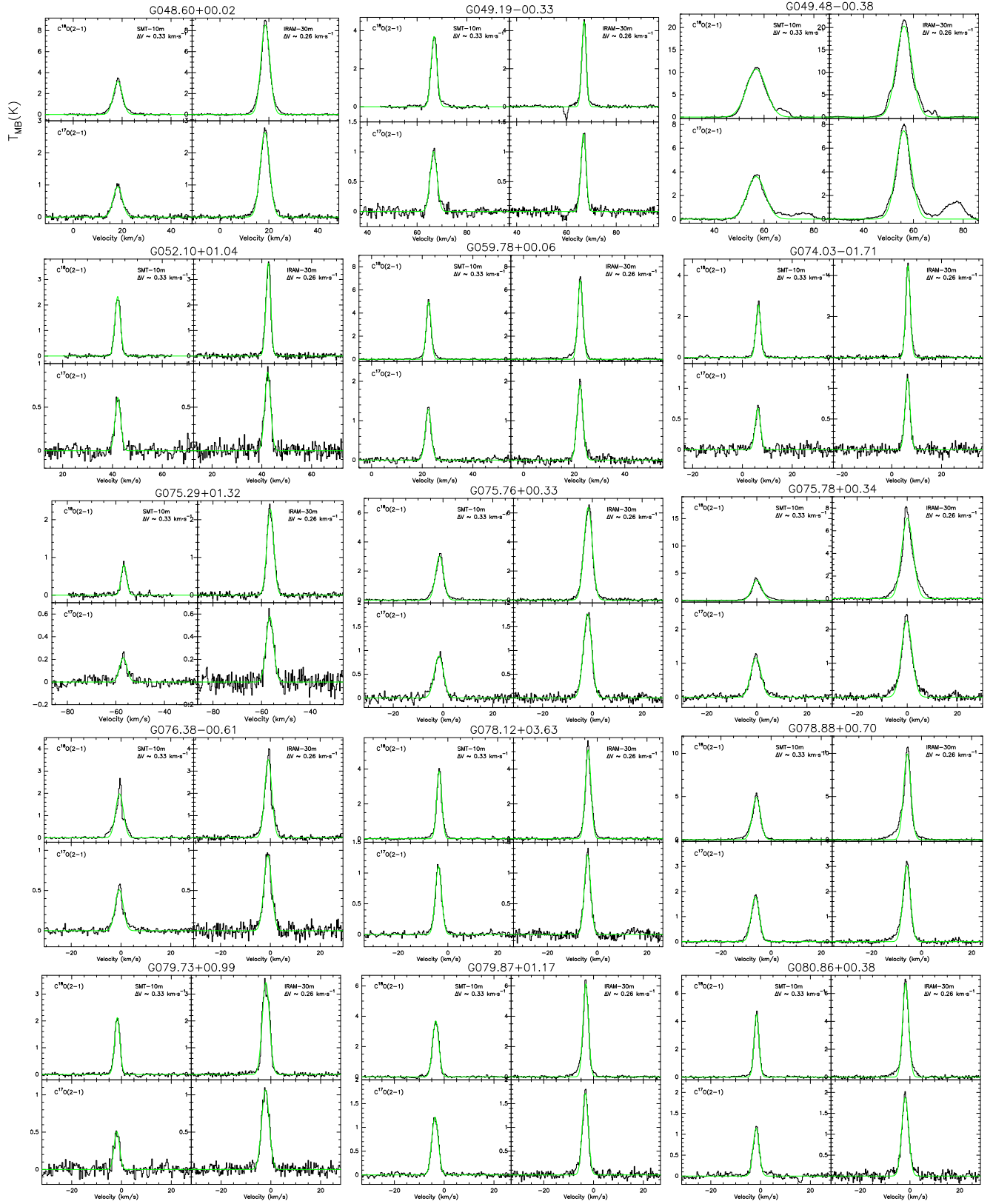


Figure 4. The spectra of $C^{18}O$ (upper panels) and $C^{17}O$ (lower panels) with green fit lines of those 41 sources detected by both the SMT 10 m (left columns) and the IRAM 30 m (right columns) telescopes. (An extended version of this figure is available).

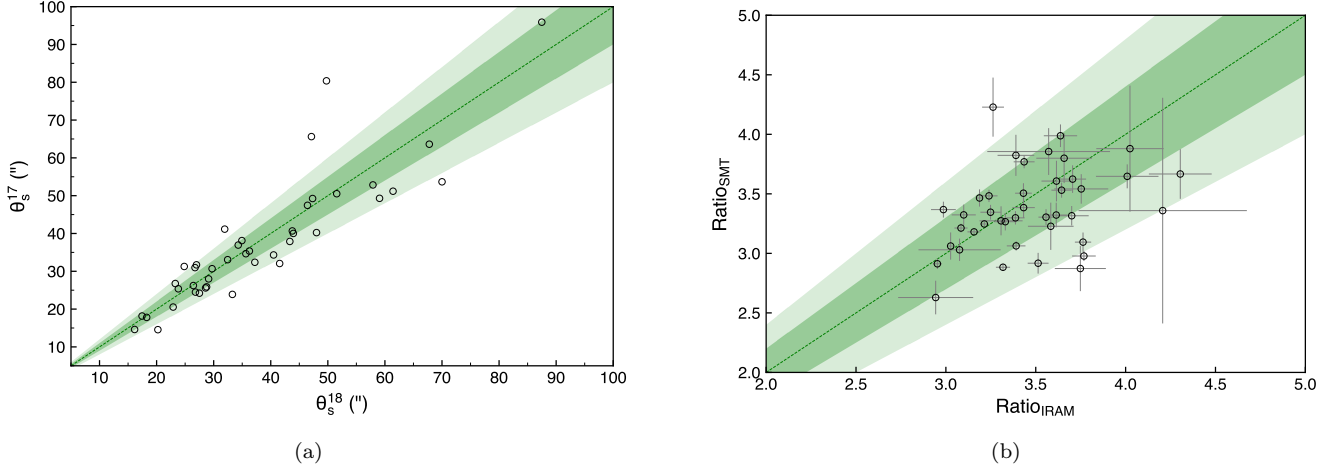


Figure 5. The comparison of estimated source sizes from C¹⁸O and C¹⁷O J=2-1 lines (left panel) and the isotope ratio measured by IRAM 30 m and SMT 10 m (right panel) for those 41 sources detected by both telescopes toward identical positions. The green dashed lines indicate $\theta_s^{18} = \theta_s^{17}$ and $\text{Ratio}_{\text{IRAM}} = \text{Ratio}_{\text{SMT}}$, while the dark and light green shaded areas indicate the $\pm 10\%$ and $\pm 20\%$ error ranges, respectively.

within an error range of 20% (see green shaded regions). Figure 5(b) compares measured ¹⁸O/¹⁷O ratios from both telescopes. It shows that the measured ratios by both telescopes are mostly consistent ($\sim 90\%$ sources, 37 out of 41), within a 20% error range. To summarize, any observational bias is not significant with respect to our resulting ¹⁸O/¹⁷O isotope ratios.

Table 2. A comparison of IRAM 30 m and SMT 10 m results for the 41 common sources with C¹⁸O and C¹⁷O detections.

Source Name	R.A.	Decl.	R_{GC}	d	Telescope	Line	rms	V_{peak}	$\int T_{mb} d\nu$	T_{peak}	$Ratio_{corr}$
	(J2000)	(J2000)	(kpc)	(kpc)			(mK)	(km s ⁻¹)	(K km s ⁻¹)	(K)	
(1)	(2)	(3)	(4)	(5)	(6)	(7)	(8)	(9)	(10)	(11)	(12)
G121.29+00.65	00 36 47.3	63 29 02.18	8.86	0.93	IRAM	C ¹⁸ O	35	-17.50 (0.01)	14.16 (0.06)	5.17	3.24 (0.05)
					IRAM	C ¹⁷ O	43	-17.74 (0.02)	4.58 (0.06)	1.43	
					SMT	C ¹⁸ O	36	-17.48 (0.01)	10.45 (0.07)	3.95	3.48 (0.05)
					SMT	C ¹⁷ O	25	-17.66 (0.02)	3.14 (0.04)	1.00	
G122.01-07.08	00 44 58.4	55 46 47.60	9.67	2.17	IRAM	C ¹⁸ O	32	-50.21 (0.00)	12.65 (0.05)	4.80	3.08 (0.23)
					IRAM	C ¹⁷ O	34	-51.37 (0.07)	4.30 (0.33)	1.47	
					SMT	C ¹⁸ O	44	-50.83 (0.01)	10.02 (0.05)	4.15	3.03 (0.09)
					SMT	C ¹⁷ O	76	-51.03 (0.04)	3.46 (0.11)	1.25	
G123.06-06.30a	00 52 24.7	56 33 50.51	10.15	2.82	IRAM	C ¹⁸ O	43	-30.30 (0.01)	14.28 (0.08)	3.86	3.64 (0.06)
					IRAM	C ¹⁷ O	42	-30.58 (0.03)	4.10 (0.06)	1.08	
					SMT	C ¹⁸ O	29	-30.44 (0.01)	10.33 (0.05)	2.82	3.53 (0.06)
					SMT	C ¹⁷ O	26	-30.78 (0.03)	3.06 (0.05)	0.76	
WB89 382	01 08 49.5	62 33 14.00	11.31	4.04	IRAM	C ¹⁸ O	78	-43.61 (0.01)	3.33 (0.07)	2.47	3.57 (0.34)
					IRAM	C ¹⁷ O	80	-43.74 (0.10)	0.98 (0.09)	0.40	
					SMT	C ¹⁸ O	41	-43.78 (0.01)	3.01 (0.04)	1.92	3.86 (0.20)
					SMT	C ¹⁷ O	33	-43.85 (0.05)	0.82 (0.04)	0.36	
G133.94+01.06	02 27 03.8	61 52 25.21	9.80	1.95	IRAM	C ¹⁸ O	36	-47.24 (0.02)	32.75 (0.06)	6.58	3.03 (0.02)
					IRAM	C ¹⁷ O	37	-47.57 (0.01)	11.33 (0.06)	2.14	

Table 2 continued on next page

Table 2 (continued)

Source Name	R.A.	Decl.	R_{GC}	d	Telescope	Line	rms	V_{peak}	$\int T_{mb} d\nu$	T_{peak}	$Ratio_{corr}$
(1)	(J2000)	(J2000)	(kpc)	(kpc)	(6)	(7)	(mK)	(km s $^{-1}$)	(K km s $^{-1}$)	(K)	(12)
					SMT	C 18 O	69	-47.32 (0.01)	28.39 (0.12)	6.01	3.06 (0.11)
					SMT	C 17 O	63	-47.87 (0.09)	9.71 (0.36)	1.98	

NOTE—Column (1): source name. Columns (2) and (3): equatorial J2000 coordinates. Column (4): the galactocentric distance R_{GC} . Column (5): the heliocentric distance d . Column (6): telescopes used. Column (7): molecular species. Column (8): the rms (velocity resolutions are the same as in Table 1) value in units of T_{mb} . Column (9): the velocity of the peak T_{mb} . Column (10): the integrated intensities of C 18 O and C 17 O with standard deviation errors in parentheses. Column (11): the line peak values in T_{mb} . Column (12): the frequency-corrected abundance ratio with its error in parentheses. (This table is available in its entirety in machine-readable form.)

4.2. Galactic Interstellar $^{18}\text{O}/^{17}\text{O}$ Gradient

4.2.1. A prominent $^{18}\text{O}/^{17}\text{O}$ gradient from the $J=2-1$ lines of C ^{18}O and C ^{17}O

With the IRAM 30 m and the SMT 10 m measurements of C ^{18}O and C ^{17}O $J=2-1$, we obtained $^{18}\text{O}/^{17}\text{O}$ isotope ratios from 364 sources. Ratios are plotted against their galactocentric distances in Figure 6(a). As in the case of our $J = 1-0$ results (see Paper I), we find rising $^{18}\text{O}/^{17}\text{O}$ ratios with increasing galactocentric distance, though there is significant scatter, especially for the SMT 10 m measurements. In order to show the trend more clearly, we average our results in bins of 1 kpc in galactocentric distance for both the SMT 10 m and the IRAM 30 m sample. The bin-averaged ratios are plotted as a function of galactocentric distance in Figure 6(b). Apparently, both data sets show similar gradients, i.e., the $^{18}\text{O}/^{17}\text{O}$ ratios are smaller near the GC and larger in the outskirts of the Galaxy.

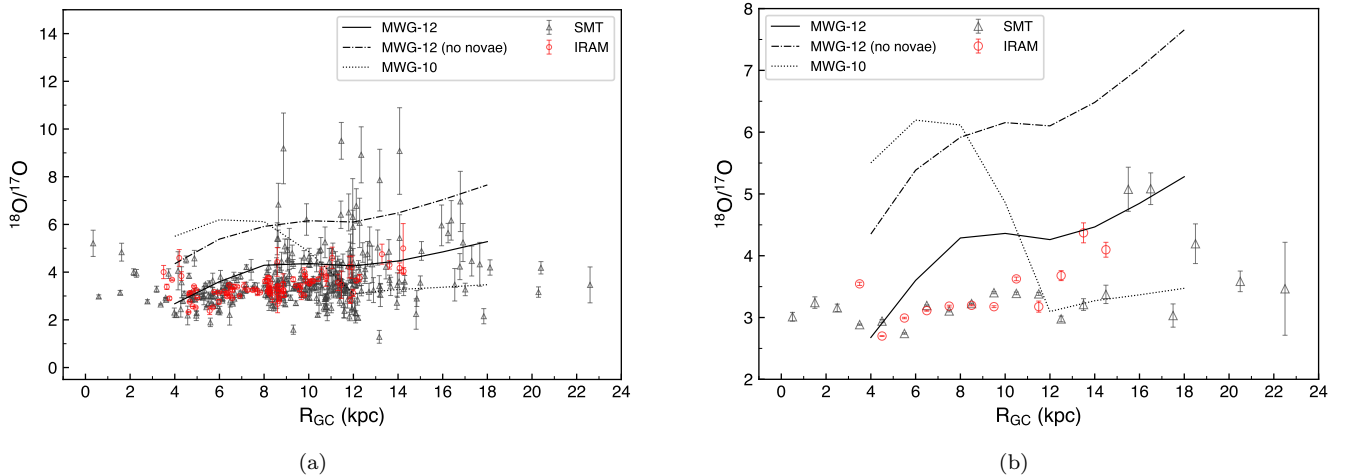


Figure 6. $^{18}\text{O}/^{17}\text{O}$ isotope ratios plotted as a function of galactocentric distance, R_{GC} (Figure 6(a), left panel). In Figure 6(b) (right panel), we plot the weighted average values (weight $1/\sigma^2$, see Paper I) of the ratio in bins of 1 kpc in R_{GC} . The red circles and black triangles are the results from our IRAM 30 m and SMT 10 m measurements, respectively. The curves represent predictions of the most recent galactic chemical evolution model; the dotted curve represents the model adopting the new yields by Limongi & Chieffi (2018) for non-rotating stars (MWG-10), the dash-dotted and solid curves are for rotating stars without or with novae, respectively (MWG-12; see details in Romano et al. 2019).

Only accounting for the HMSFR subsample with accurate distance values, measured by trigonometric parallaxes making use of maser lines (Reid et al. 2014; Reid et al. 2019), statistical results should be particularly reliable. In addition, IRAM 30 m measurements should be more accurate, thanks to the wide bandwidth (both C ^{18}O and C ^{17}O

line were observed simultaneously) and smaller beam size (less beam dilution, leading to higher line temperatures and signal-to-noise ratios), which minimizes observational effects (see details in Section 4.1). Thus we took the HMSFR sample with parallax distances and IRAM 30 m measurements to determine accurately the $^{18}\text{O}/^{17}\text{O}$ gradient in terms of the galactocentric distance. This subsample contains 72 sources, covering a galactocentric distance range of 3-14 kpc. Their $^{18}\text{O}/^{17}\text{O}$ ratios as a function of galactocentric distance are plotted in Figure 7. In contrast to the large scatter for the entire sample (Figure 6(a)), Figure 7 shows the correlation of $^{18}\text{O}/^{17}\text{O}$ with galactocentric distance more clearly. The unweighted linear fit provides a radial gradient of the ratio, $^{18}\text{O}/^{17}\text{O} = (0.12 \pm 0.02)R_{\text{GC}} + (2.38 \pm 0.13)$, with a Pearson’s rank correlation coefficient of $R = 0.67$. We also present the bin-averaged results from our J=1-0 measurements (Paper I) in Figure 7. Our results from both J=1-0 and J=2-1 data show identically one significant correlation between the ratio and the galactocentric distance, with the same slope for both fit lines (Figure 7). In addition we find that ratios from the J=2-1 lines tend to be systematically smaller than those from the J=1-0 data. For those 142 sources with measured ratios from J=1-0 and J=2-1 data, the ratio from J=1-0 data (Ratio₁₋₀) is mostly larger than that from J=2-1 data (Ratio₂₋₁; see Figure 8) in $\sim 80\%$ of the sources. The difference in the measured ratios from the two transitions will be discussed in the subsection 4.2.2.

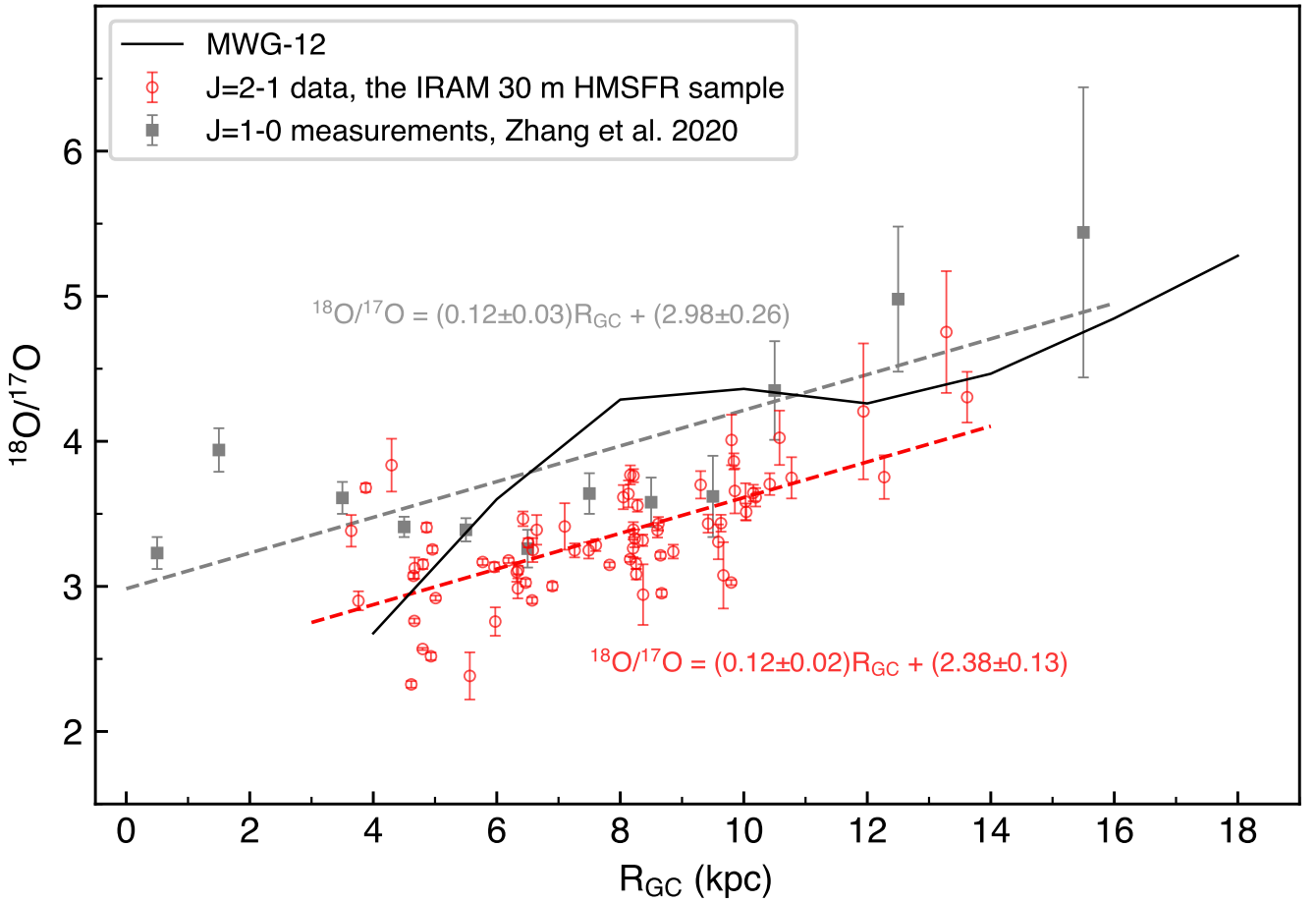


Figure 7. A prominent radial $^{18}\text{O}/^{17}\text{O}$ gradient is confirmed by our HMSFR sample, encompassing 72 sources with accurate distance values. Red and grey colors are used to indicate the results from J=2-1 and J=1-0 data (the latter taken from Paper I), respectively. The dashed lines represent unweighted linear fits, while the expressions give the fitting parameters. As in Figure 6(a), the curve represents predictions of the GCE model including both rotating stars and novae (MWG-12 in Romano et al. 2019).

Modeling works on galactic chemical evolution (GCE) can certainly help us to better understand the galactic radial gradient of $^{18}\text{O}/^{17}\text{O}$. Similar to Paper I, modeling results from the latest theoretical works (Romano et al. 2019) are

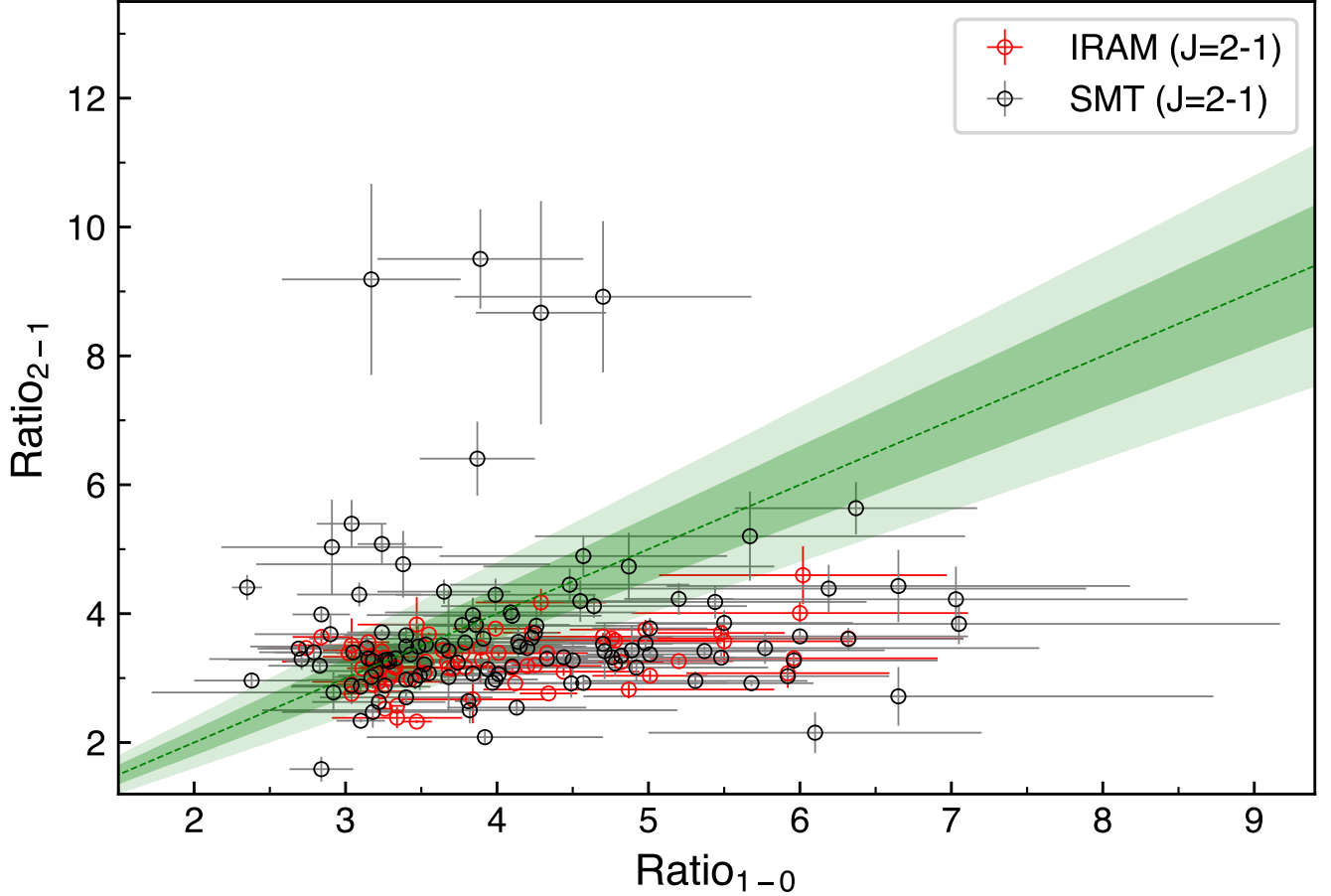


Figure 8. A comparison of isotope ratios from our J=1-0 (Paper I) and J=2-1 (this paper) data. Red and grey colors indicate IRAM and SMT J=2-1 data, respectively. For the green line and shaded areas, see the caption to Figure 5.

shown in Figure 6(a) and Figure 7 (solid, dotted and dashed-dotted curves), including MWG-10 (massive stars without fast rotation), MWG-12 (including both rotating massive stars and novae) and MWG-12nn (including rotating massive stars, but no nova contribution). As shown in Figure 6(a) and Figure 7, MWG-12 can match best our measurements, i.e., including contributions from both fast rotating massive stars and novae. Contributions from fast rotators can provide high $^{18}\text{O}/^{17}\text{O}$ ratios in the outer, metal-poor Galactic disk, which plays a unique role in the positive gradient of $^{18}\text{O}/^{17}\text{O}$ (e.g., Frischknecht et al. 2016). And the contribution of nova nucleosynthesis should not be neglected, although it still involves many uncertainties (Romano et al. 2017). Large variations of the individual nova yields coupled to the rarity of nova outbursts may be partly responsible for the scatter presented in our data. However, the difference between the J=2-1 data and the modeling results is larger than the corresponding difference related to the J=1-0 results (see Figure 7). This may be caused by the larger optical depth of the C^{18}O J=2-1 lines, which will be discussed in the next subsection.

4.2.2. Comparison of J=2-1 and J=1-0 measurements

In Section 4.2.1, we found that the ratios from J=2-1 data tend to be systematically lower than those from the J=1-0 measurements and those from modeling (MWG-12, Figure 7). This is probably related to the optical depths of the C^{18}O J=2-1 lines. The optical depth of the C^{17}O line can be directly determined by fitting its hyperfine structure lines (see details in Paper I), and then we can get the optical depth of the C^{18}O line, assuming that it is about four times that of the corresponding C^{17}O line. However, the velocity differences between the hyperfine components of our C^{17}O J=2-1 lines ($\sim 1.2 \text{ km s}^{-1}$) is in most cases too small to be spectroscopically resolvable, thus leading to unreliable results. As substitution, a qualitative analysis to test for saturation effects of C^{18}O was made by making

use of the more abundant isotopic species ¹³CO, whose J=2-1 line was also covered by our IRAM 30 m observations. Apparently, any source in which the intensity of the C¹⁸O line is reduced by opacity effects can be expected to present a correspondingly greater diminution in its ¹³CO spectrum. Thus, we can expect the greatest saturation effects in the C¹⁸O/C¹⁷O ratios in those sources showing the lowest ¹³CO/C¹⁸O line intensity ratios (Penzias 1981). ¹³CO/C¹⁸O against C¹⁸O/C¹⁷O is presented in Figure 9 and we can find that small ¹³CO/C¹⁸O ratios are associated with small C¹⁸O/C¹⁷O values. This implies that our measured C¹⁸O J=2-1 lines are to some degree saturated.

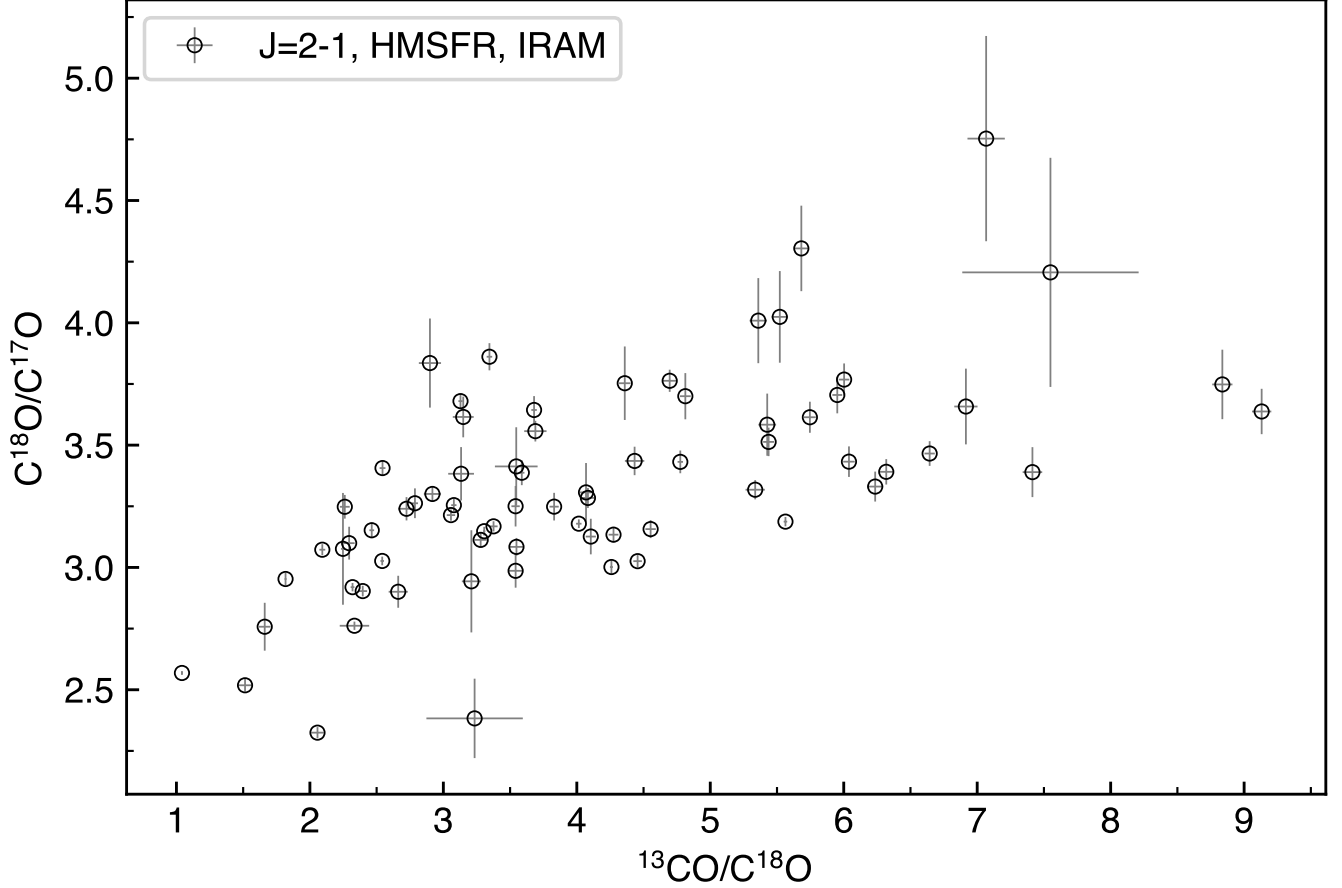


Figure 9. The C¹⁸O/C¹⁷O integrated intensity ratio as a function of ¹³CO/C¹⁸O for the J=2-1 transition.

For those 142 sources with both Ratio₁₋₀ and Ratio₂₋₁, we plotted Ratio₁₋₀/Ratio₂₋₁ as a function of Ratio₁₋₀ in Figure 10. We can find that the Ratio₁₋₀/Ratio₂₋₁ slowly increases with Ratio₁₋₀, which means that in absolute but not in relative terms (e.g., Section 4.2.1 and Figure 7) Ratio₂₋₁ has a lower increasing rate than Ratio₁₋₀. This suggests a more pronounced saturation in the C¹⁸O J=2-1 line with regard to the C¹⁸O J=1-0 line and thus the real abundance ratio may be underestimated by our analysis of the J=2-1 lines. Therefore, it is necessary to check the degree of saturation in the C¹⁸O J=2-1 line and assess its possible effect on the ratio results.

In order to give a quantitative estimation of the saturation effect, we performed a non-LTE analysis for the C¹⁸O J=2-1 line using the RADEX software (van der Tak et al. 2007) toward our sample. We cross-matched our sample with the published ATLASGAL catalogue (Billington et al. 2019) and obtained $n(\text{H}_2)$ data for 24 sources. The kinetic temperatures of these 24 sources were also collected (Milam et al. 2005; Hill et al. 2010; Dunham et al. 2011; Urquhart et al. 2011; Wiene et al. 2012; Cyganowski et al. 2013; Svoboda et al. 2016; Billington et al. 2019; Chen et al. 2021; Wiene et al. 2021). With $n(\text{H}_2)$, T_k , molecular data from the Leiden Atomic and Molecular Database⁴ (LAMDA)

⁴ <https://home.strw.leidenuniv.nl/moldata/>

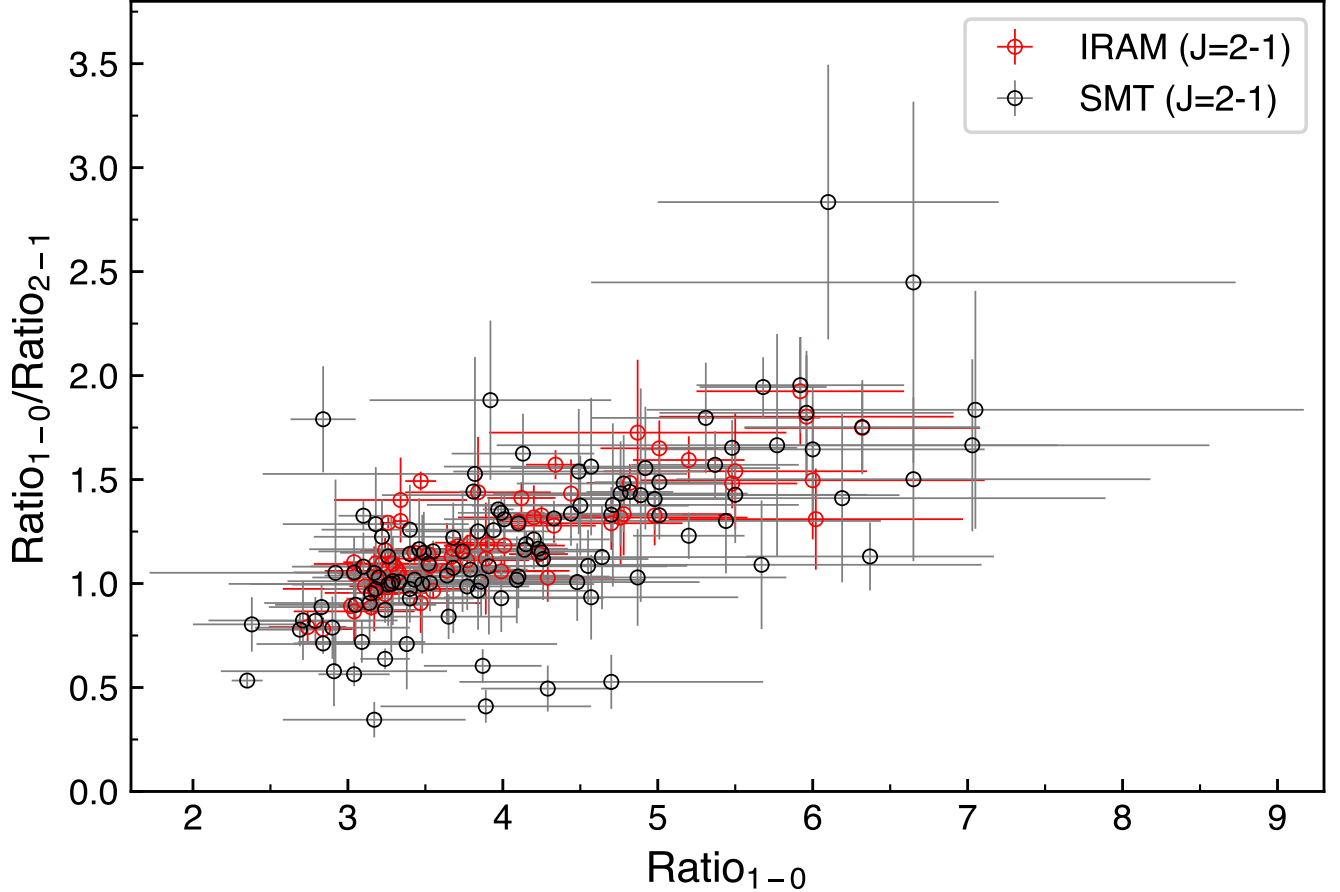


Figure 10. The $\text{Ratio}_{1-0}/\text{Ratio}_{2-1}$ values are plotted as a function of Ratio_{1-0} . Red and grey colors indicate IRAM and SMT J=2-1 data, respectively.

and our spectral line data, we performed RADEX calculations and obtained the optical depths for the C^{18}O J=2-1 lines. It ranges from 0.1 to 2.0, mostly (>80%) less than 1.0, with an average value of ~ 0.5 (corresponding correction of $\sim 20\%$ on the ratio). This indicates that in some cases C^{18}O J=2-1 is saturated, but overall the opacity effect should be moderate. For comparison, we also calculated the optical depths of the C^{18}O J=1-0 line for those 24 sources. With regard to the C^{18}O 2-1 line, smaller optical depths were obtained for the J=1-0 transition, with an average optical depth of ~ 0.1 (corresponding correction of $\sim 4\%$), which agrees with results in [Paper I](#), i.e., non-significant optical depth effects for the J=1-0 line. After correcting for the optical depth effect in both lines, we find that the ratio results measured by both J=2-1 and J=1-0 transitions are consistent within errors (see [Figure 11\(b\)](#)).

5. SUMMARY

We are performing systematic observations of multi-transition lines of C^{18}O and C^{17}O toward a large sample of molecular clouds in the Galaxy, covering the Galactic plane from the central region to the far outer Galaxy (~ 22 kpc), to search for variations in the oxygen $^{18}\text{O}/^{17}\text{O}$ isotope ratio as a function of galactocentric distance. In this work, we present a large C^{18}O and C^{17}O J=2-1 survey, observed with the IRAM 30 m and the SMT 10 m telescopes. 96 out of 103 sources were successfully detected in both C^{18}O and C^{17}O J=2-1 lines through the IRAM 30 m, while 325 out of 380 sources were detected in both lines using the SMT 10 m. 62 sources were observed by both telescopes, 41 of them were detected toward exactly the same position in both C^{18}O and C^{17}O J=2-1, which is used to check the quality of the data and to evaluate beam dilution. Our main results are as follows:

(1) From the measured J=2-1 line intensities, $^{18}\text{O}/^{17}\text{O}$ ratios could be obtained for 364 sources. No systematic variation is found between the isotopic ratio and the heliocentric distance, which implies that any observational bias due to beam dilution is not significant. We analyzed observational data from those sources detected by both the

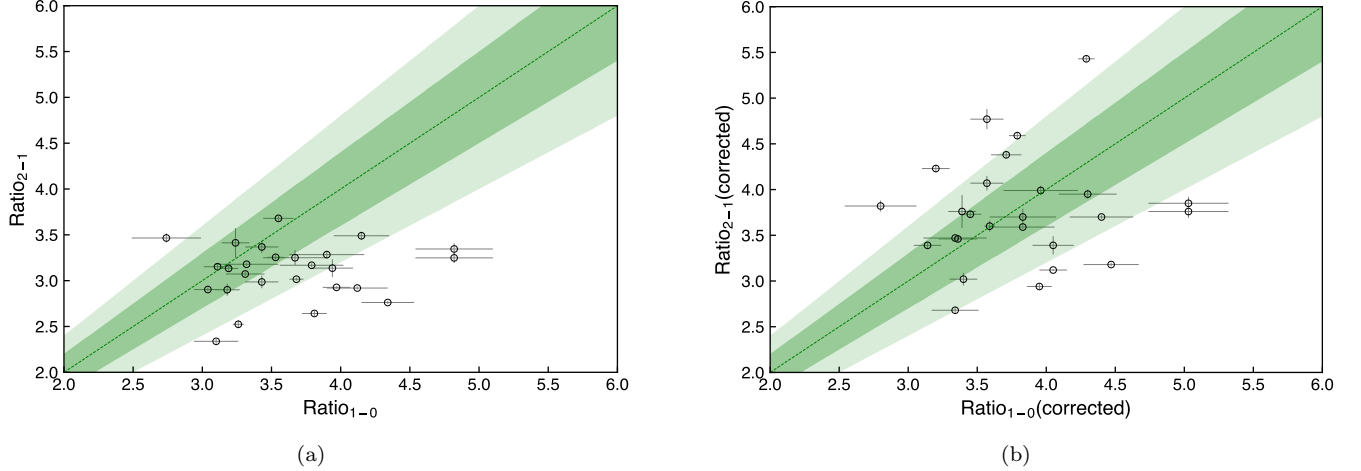


Figure 11. A comparisons of the $^{18}\text{O}/^{17}\text{O}$ ratios from our J=1-0 and J=2-1 data for 24 sources. Left and right panel are before and after correction of RADEX calculations, respectively. The green line and shaded areas are similar as Figure 5.

SMT 10 m and IRAM 30 m telescopes, derived source sizes and obtained consistent $^{18}\text{O}/^{17}\text{O}$ isotope ratios. This also implies that linear resolution and beam dilution do not significantly affect the determined isotope ratios.

(2) The measured $^{18}\text{O}/^{17}\text{O}$ isotope ratios of 364 sources tend to increase with galactocentric distance, though the scatter is large. The gradient is most clearly seen in the subsample of high-mass star-forming regions (HMSFRs) detected with the IRAM 30 m telescope. These data are characterized by high signal-to-noise ratios and are also the least affected by observational effects. The unweighted linear fit determines the radial gradient as $^{18}\text{O}/^{17}\text{O} = (0.12 \pm 0.02)R_{GC} + (2.38 \pm 0.13)$, with a Pearson’s rank correlation coefficient of $R = 0.67$. This is consistent with prediction by a recent model of Galactic chemical evolution, considering contributions from both fast rotating massive stars and novae. The randomness of the latter’s yield may cause a part of the scatter revealed by our data.

(3) Our measured $^{18}\text{O}/^{17}\text{O}$ ratios from the C¹⁸O and C¹⁷O J=2-1 lines (Ratio_{2-1}) tend to be lower than those from the J=1-0 lines (Ratio_{1-0}), though both present identical trends of increasing $^{18}\text{O}/^{17}\text{O}$ ratios with rising galactocentric distance. The difference is likely caused by the fact that in many instances the C¹⁸O J=2-1 line is not optically thin. This is supported by the positive correlation between $\text{Ratio}_{1-0}/\text{Ratio}_{2-1}$ and Ratio_{1-0} , and the RADEX non-LTE model calculation results, which suggest average optical depths of about 0.5 and 0.1 for C¹⁸O J=2-1 and 1-0, respectively. After optical depth correction, consistent $^{18}\text{O}/^{17}\text{O}$ ratio can be obtained within the limits of observational accuracy.

ACKNOWLEDGMENTS

1
2 This work is supported by the National Key R&D program of China (2022YFA1603102) and the Natural Science
3 Foundation of China (No. 12373021, 12041302, 11590782). D.R. thanks the Italian National Institute for Astrophysics
4 (INAF) for the support provided to the project “*An in-depth theoretical study of CNO element evolution in galaxies*”
5 via Theory Grant 2022, Fu. Ob. 1.05.12.06.08. We thank the operators and staff at both IRAM 30 m and SMT 10 m
6 stations for their assistance during our observations.

APPENDIX

The spectra of the targets that were not detected (or with only hints of a detection, which are candidates for additional observation) are shown in Figure A1.

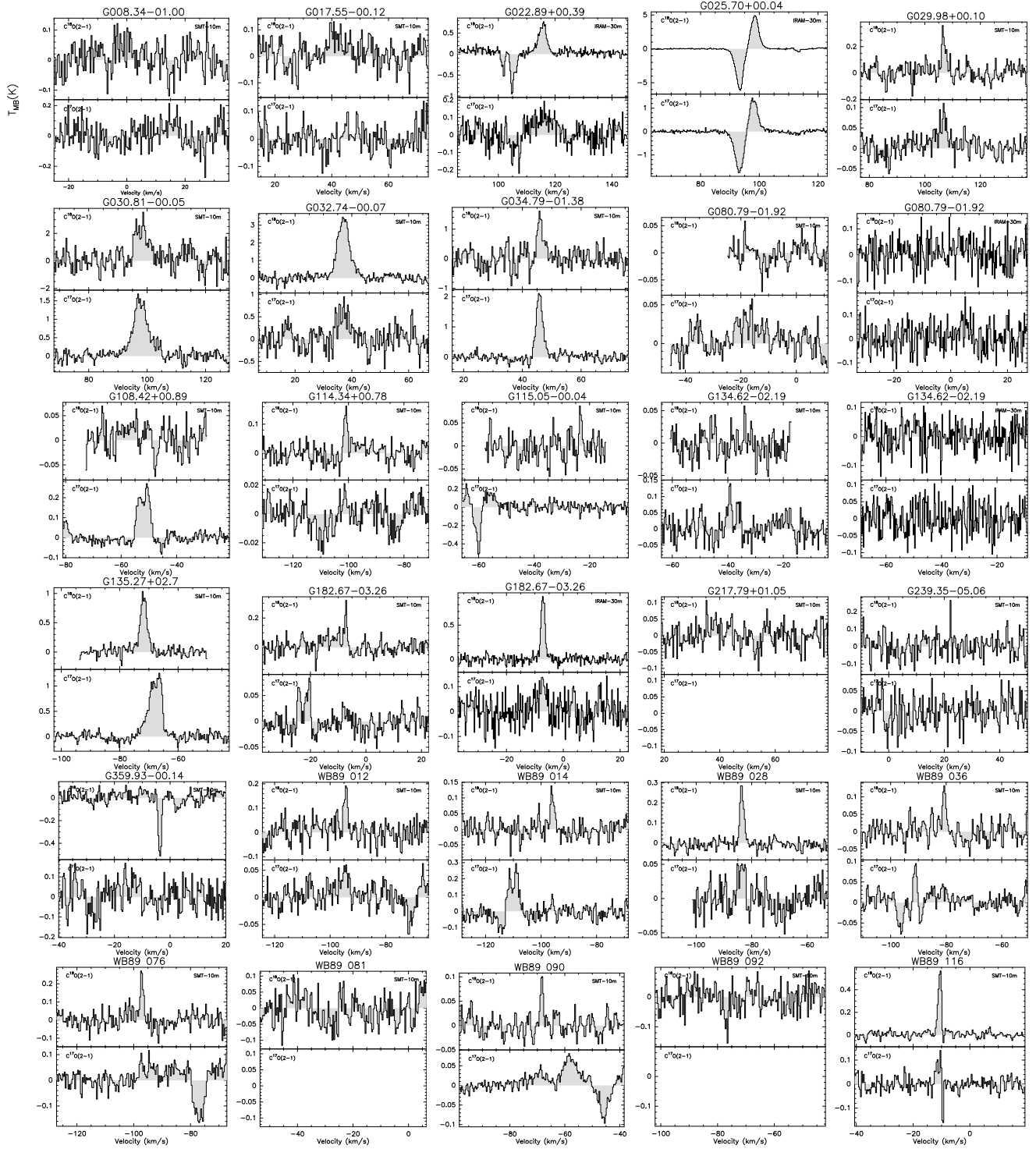


Figure A1. Spectra of those sources without effective measurements of $C^{18}O/C^{17}O$.
(An extended version of this figure is available).

REFERENCES

- Bensch, F., Pak, I., Wouterloot, J. G. A., Klapper, G., & Winnewisser, G. 2001, *ApJL*, 562, L185, doi: [10.1086/338253](https://doi.org/10.1086/338253)
- Billington, S. J., Urquhart, J. S., König, C., et al. 2019, *MNRAS*, 490, 2779, doi: [10.1093/mnras/stz2691](https://doi.org/10.1093/mnras/stz2691)
- Chen, J. L., Zhang, J. S., Henkel, C., et al. 2021, *ApJS*, 257, 39, doi: [10.3847/1538-4365/ac205a](https://doi.org/10.3847/1538-4365/ac205a)
- Cyganowski, C. J., Koda, J., Rosolowsky, E., et al. 2013, *ApJ*, 764, 61, doi: [10.1088/0004-637X/764/1/61](https://doi.org/10.1088/0004-637X/764/1/61)
- Dunham, M. K., Rosolowsky, E., Evans, Neal J., I., Cyganowski, C., & Urquhart, J. S. 2011, *ApJ*, 741, 110, doi: [10.1088/0004-637X/741/2/110](https://doi.org/10.1088/0004-637X/741/2/110)
- Esteban, C., & Garc í a-Rojas, J. 2018, *MNRAS*, 478, 2315, doi: [10.1093/mnras/sty1168](https://doi.org/10.1093/mnras/sty1168)
- Frischknecht, U., Hirschi, R., Pignatari, M., et al. 2016, *MNRAS*, 456, 1803, doi: [10.1093/mnras/stv2723](https://doi.org/10.1093/mnras/stv2723)
- Henry, R. B. C., Kwitter, K. B., Jaskot, A. E., et al. 2010, *ApJ*, 724, 748, doi: [10.1088/0004-637X/724/1/748](https://doi.org/10.1088/0004-637X/724/1/748)
- Hill, T., Longmore, S. N., Pinte, C., et al. 2010, *MNRAS*, 402, 2682, doi: [10.1111/j.1365-2966.2009.16101.x](https://doi.org/10.1111/j.1365-2966.2009.16101.x)
- Humire, P. K., Thiel, V., Henkel, C., et al. 2020, *A&A*, 642, A222, doi: [10.1051/0004-6361/202038216](https://doi.org/10.1051/0004-6361/202038216)
- Ladd, E. F. 2004, *ApJ*, 610, 320, doi: [10.1086/421387](https://doi.org/10.1086/421387)
- Larson, R. B. 1976, *MNRAS*, 176, 31, doi: [10.1093/mnras/176.1.31](https://doi.org/10.1093/mnras/176.1.31)
- Li, H.-K., Zhang, J.-S., Liu, Z.-W., et al. 2016, *Research in Astronomy and Astrophysics*, 16, 47, doi: [10.1088/1674-4527/16/3/047](https://doi.org/10.1088/1674-4527/16/3/047)
- Limongi, M., & Chieffi, A. 2018, *ApJS*, 237, 13, doi: [10.3847/1538-4365/aacb24](https://doi.org/10.3847/1538-4365/aacb24)
- Milam, S. N., Savage, C., Brewster, M. A., Ziurys, L. M., & Wyckoff, S. 2005, *ApJ*, 634, 1126, doi: [10.1086/497123](https://doi.org/10.1086/497123)
- Penzias, A. A. 1981, *ApJ*, 249, 518, doi: [10.1086/159311](https://doi.org/10.1086/159311)
- Reid, M. J., Menten, K. M., Brunthaler, A., et al. 2014, *ApJ*, 783, 130, doi: [10.1088/0004-637X/783/2/130](https://doi.org/10.1088/0004-637X/783/2/130)
- Reid, M. J., Menten, K. M., Brunthaler, A., et al. 2019, *ApJ*, 885, 131, doi: [10.3847/1538-4357/ab4a11](https://doi.org/10.3847/1538-4357/ab4a11)
- Romano, D., Matteucci, F., Zhang, Z.-Y., Ivison, R. J., & Ventura, P. 2019, *MNRAS*, 490, 2838, doi: [10.1093/mnras/stz2741](https://doi.org/10.1093/mnras/stz2741)
- Romano, D., Matteucci, F., Zhang, Z. Y., Papadopoulos, P. P., & Ivison, R. J. 2017, *Monthly Notices of the Royal Astronomical Society*, 470, 401, doi: [10.1093/mnras/stx1197](https://doi.org/10.1093/mnras/stx1197)
- Svoboda, B. E., Shirley, Y. L., Battersby, C., et al. 2016, *ApJ*, 822, 59, doi: [10.3847/0004-637X/822/2/59](https://doi.org/10.3847/0004-637X/822/2/59)
- Urquhart, J. S., Morgan, L. K., Figura, C. C., et al. 2011, *MNRAS*, 418, 1689, doi: [10.1111/j.1365-2966.2011.19594.x](https://doi.org/10.1111/j.1365-2966.2011.19594.x)
- van der Tak, F. F. S., Black, J. H., Schöier, F. L., Jansen, D. J., & van Dishoeck, E. F. 2007, *A&A*, 468, 627, doi: [10.1051/0004-6361:20066820](https://doi.org/10.1051/0004-6361:20066820)
- Wienen, M., Wyrowski, F., Schuller, F., et al. 2012, *A&A*, 544, A146, doi: [10.1051/0004-6361/201118107](https://doi.org/10.1051/0004-6361/201118107)
- Wienen, M., Wyrowski, F., Walmsley, C. M., et al. 2021, *A&A*, 649, A21, doi: [10.1051/0004-6361/201731208](https://doi.org/10.1051/0004-6361/201731208)
- Wilson, T. L., & Rood, R. 1994, *ARA&A*, 32, 191, doi: [10.1146/annurev.aa.32.090194.001203](https://doi.org/10.1146/annurev.aa.32.090194.001203)
- Wouterloot, J. G. A., & Brand, J. 1989, *A&AS*, 80, 149
- Wouterloot, J. G. A., Brand, J., & Henkel, C. 2005, *A&A*, 430, 549, doi: [10.1051/0004-6361:20040437](https://doi.org/10.1051/0004-6361:20040437)
- Wouterloot, J. G. A., Henkel, C., Brand, J., et al. 2008, *A&A*, 487, 237, doi: [10.1051/0004-6361:20078156](https://doi.org/10.1051/0004-6361:20078156)
- Xiang, M.-S., Liu, X.-W., Shi, J.-R., et al. 2017, *MNRAS*, 464, 3657, doi: [10.1093/mnras/stw2523](https://doi.org/10.1093/mnras/stw2523)
- Yan, Y. T., Zhang, J. S., Henkel, C., et al. 2019, *ApJ*, 877, 154, doi: [10.3847/1538-4357/ab17d6](https://doi.org/10.3847/1538-4357/ab17d6)
- Yan, Y. T., Henkel, C., Kobayashi, C., et al. 2023, *A&A*, 670, A98, doi: [10.1051/0004-6361/202244584](https://doi.org/10.1051/0004-6361/202244584)
- Yu, H. Z., Zhang, J. S., Henkel, C., et al. 2020, *ApJ*, 899, 145, doi: [10.3847/1538-4357/aba8f1](https://doi.org/10.3847/1538-4357/aba8f1)
- Zhang, J. S., Henkel, C., Mauersberger, R., et al. 2007, *A&A*, 465, 887, doi: [10.1051/0004-6361:20065931](https://doi.org/10.1051/0004-6361:20065931)
- Zhang, J. S., Sun, L. L., Riquelme, D., et al. 2015, *ApJS*, 219, 28, doi: [10.1088/0067-0049/219/2/28](https://doi.org/10.1088/0067-0049/219/2/28)
- Zhang, J. S., Liu, W., Yan, Y. T., et al. 2020, *ApJ Supplement Series*, 249, 6, (Paper I), doi: [10.3847/1538-4365/ab9112](https://doi.org/10.3847/1538-4365/ab9112)